OPTIMIZATION OF JETTED MULTI-LATERAL WELL DESIGN

Elisabeth Peters[1], Diederik Troost[2], Olwijn Leeuwenburgh[1,2]

[1] TNO, Utrecht, The Netherlands

[2] Delft University of Technology, Delft, The Netherlands

lies.peters@tno.nl

Keywords: radial jet drilling, optimization, CMA-ES.

ABSTRACT

Geothermal wells can be stimulated to increase productivity or injectivity by drilling multiple, small-diameter laterals using a technique called Radial Jet Drilling (RJD). Laterals can be freely placed along a backbone well, making an optimal distribution of laterals over the backbone or well design time intensive. Therefore numerical optimization will be applied for the design. Because of the discrete nature of the optimization problem, the gradient-free CMA-ES algorithm is chosen for the optimisation. Also an uncertainty-handling CMA-ES is incorporated in the workflow, because the jetting process us not steered and thus the lateral path is uncertain. Two case studies are evaluated for optimization using these algorithms. The first is a reservoir with two high permeability layers with a vertical well. The second case is a vertical well in a fine-layered reservoir. For both cases, the number and depth of the laterals is optimized. The workflow is able to determine well plans with higher NPV in each of these cases, although finding a global optimum remains difficult.

1. INTRODUCTION

Geothermal wells can be stimulated to increase productivity or injectivity by drilling multiple, small-diameter laterals using a technique called Radial Jet Drilling (RJD). In this technique, multiple laterals with lengths up to 100 m and a diameter of 25 to 50 mm are created using hydraulic jetting (see e.g. Kamel, 2017, Yan et al, 2018). A common design is, for example, to jet 8 to 16 laterals in a single well in groups of 4 with a spacing between laterals at a single kickoff point of 90° (Figure 1). The kickoff points can in principle be positioned anywhere along the length of the backbone. Their positioning can therefore be chosen to achieve an optimal productivity or injectivity for the well as a whole, or for the performance of a geothermal doublet. In the presence of geological heterogeneity, the effect of alternative placings may be difficult to predict without the use of a numerical simulation model. If such a model is available, alternative placings can be tested and compared. In fact the entire design of each well can be evaluated and optimized by means of numerical optimization methods. The use of model-based optimization for field and well design has been extensively studied in the petroleum industry. Recent developments include the optimization of the trajectories of a fixed set of wells that are to be drilled from a single offshore platform (see, e.g. Barros et al., 2018). Here we are interested in investigating the possibility to find an optimal design for the RJD stimulation of a geothermal well or doublet, where the design is defined by the placement along given backbones of an unknown number of radials that are associated with some number of kickoff points. The optimality of the design will typically be determined by the difference between additional costs to drill radials and the extra revenues that are incurred as a result of the improved economic performance of the improved design.

The design parameters of the sketched optimization problem include both integers (number of laterals per kickoff, number of kickoffs) and real numbers (spacing between kickoffs and between laterals within a single kick off). The presence of integer design parameters makes the problem unsuited for solution with gradient-based methods. Here we will therefore use the Covariance Matrix Adaptation Evolutionary Strategy (CMA-ES) method from the family of population-based optimization methods.

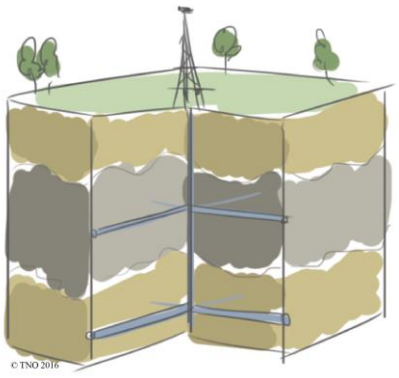

Figure 1: Conceptual illustration of a single vertical backbone and two kick-offs with four radials each spaced at 90º.

Since the laterals are not steered but rely on the stiffness of the jetting hose to keep a straight path, the actual achieved path of the laterals is uncertain. This

uncertainty should ideally be accounted for when the optimality of a particular design is evaluated. We would like to identify designs that are somewhat robust to deviations from the planned trajectories of the laterals. We will therefore investigate the use of an uncertainty-handling version of CMA-ES.

In the remainder of this paper we will define the objective function that we wish to maximize, describe the design parameters, introduce the simulation and optimization methodology, and show results of the application of the optimization workflow to two example cases of increasing complexity. The second case study is based on an existing geothermal field.

2. METHODS

2.1 Radial jetted well simulation

In order to evaluate different RJD designs, we need to be able to simulate the impact of a particular design on the flow dynamics. The inflow or outflow of each radial into the reservoir q_i is determined by the connectivity WI_i between the pressure in the radial $p_{w,i}$ and the pressure in the grid block $p_{b,i}$ in which the radial is located:

$$q_i = \frac{WI_i}{\mu}\left(p_{b,i} - p_{w,i}\right) \quad [1]$$

where μ is the viscosity of fluid. The connectivity or Well Index WI_i is computed individually for all intersections of the radial trajectory with the intersecting grid cells using the projection method or three-part Peaceman formula (Peters et al., 2018b). In this method the intersection of a well with a grid cell is projected on a local coordinate system. For each of the three projected parts, the WI is calculated which is subsequently combined into a single WI_i.

This calculation has been incorporated in a stand-alone tool based on the open source code FieldOpt (NTNU, 2018). In collaboration with NTNU, this code has been extended further to allow for well index calculation for multilateral wells.

The accuracy of this calculation is very important for the optimization. If the accuracy is insufficient, numerical errors may be larger than the differences resulting from different parameter sets. The accuracy of the projection approach was tested by comparison with the results of other simulators (Peters et al., 2018a). In addition, Troost (2019) evaluated the accuracy of the simulation, in particular the effect of changing azimuth of radials. Both studies concluded that for sufficiently fine grid (< 10 m), the error is in the order of a few percent, which is probably sufficiently small for the optimization. The calculated well indices are input for a reservoir flow simulation. All flow simulations were performed with the open-source simulator Flow that has been developed as part of the Open Porous Media (OPM) initiative (opm-project.org).

2.2 Definition of the optimization problem

In order to evaluate and compare alternative designs a performance measure needs to be determined. Here we will adopt an economic performance measure that includes the costs of drilling additional radials and the revenues associated with increased heat recovery. We define Net Present Value (NPV) of the project as

$$NPV = \sum_{t=0}^{n} \frac{P(t)}{(1+r)^t} \quad [2]$$

where $P(t)$ is the total of costs and revenues incurred at time t. The discount rate r is taken as zero in this application. Costs for radials are based on the time it takes to drill them multiplied by a day rate. Assuming a day rate of €60,000 and a drilling efficiency of 2.2. radials per day, the capital expense amounts to €27000 per radial. Revenues are proportional to the amount of heat Q produced by the laterals with $Q = m \cdot c_p \cdot \Delta T$ where m is the mass of produced water by the laterals, c_p is the heat capacity of water, and ΔT is the difference in temperature between produced water (assumed constant at 80ºC) and re-injected water (assumed to be 20ºC). The wells are operated at fixed pressure which means that the pump fuel usage depends on the flow rate only. The produced heat is translated to a monetary benefit via the price of heat (0.02 euro/kWh, 'SDE+ Basisbedrag' Lensink et al., 2018). No starting cost for the RJD job is taken into account. The costs of drilling the backbone and well operation costs do not need to be considered because only the incremental cost and benefit of the radials are included in the analysis. It should be noted that both cost and benefit contributions to the NPV are simplified and that the calculated NPV of the two case studies discussed are thus not fully representative of a real NPV for a radial jetting case.

We will now discuss the design parameters that will act as the decision variables in the optimization problem. A single, straight lateral can be characterised by the following set of parameters: kickoff depth, length, diameter, azimuth and inclination. These parameters However, to simplify the optimization, the laterals are all assumed to be 100 m long and have a fixed diameter of 0.05 m. Moreover, azimuth and inclination cannot be fully controlled and are not included in the optimization. Finally, the laterals are grouped in kick-offs. The following design parameters are therefore used per kickoff: depth (normalized from 0 to 1) and number of laterals.

2.3 Solution approach: CMA-ES

We aim to find the drilling design that maximizes the performance measure (NPV). The design is characterized here by a set of parameters. CMA-ES (Hansen and Ostermeier,1996) is a population-based optimization strategy that evaluates a set of perturbed parameters sampled from an initial distribution, ranks them according to the performance measure, updates the distribution, and samples a new set of parameters from the updated distribution. This process is repeated until convergence when the performance of the distribution mean does not improve any more. The

updates of the distribution involve separate updates of the mean m and of the covariance matrix C. The update equations are

$$m^{k+1} = \sum_{i=1}^{\mu} w_i \, x_{i:\lambda}^{k+1} \quad [3]$$

where m^{k+1} is the mean parameter vector at iteration $k+1$, based on weighting by weights w_i of the best μ members of the population that consists in total of λ members x_i,

$$p^{k+1} = (1-c_c)p^k + \sqrt{c_c(2-c_c)\mu_{eff}}\,\frac{m^{k+1}-m^k}{\sigma^k} \quad [4]$$

where p^k is the so-called evolution path vector, and all other variables are tuning parameters, and

$$C^{k+1} = (1-c_1)C^k + c_2 p^{k+1} p^{k+1^T} + c_3 \sum_{i=1}^{\mu} w_i \, y_{i:\lambda}^{k+1} y_{i:\lambda}^{k+1^T} \quad [5]$$

where $y_{i:\lambda}^{k+1}$ is a normalized member of the population at iteration k. The second and third terms in Eq. [5] are referred to as the rank-one and rank-μ updates respectively. Once a new mean and covariance matrix are determined, new samples can be generated from the resulting Gaussian distribution as characterized by the new mean and covariance matrix. Default values exist for all tuning parameters of the CMA-ES algorithm. We have adopted the values proposed by Hansen (2006).

In this work we apply one variation of the generic CMA-ES algorithm. We introduce some modifications that allow us to handle uncertainty (Hansen et al., 2009) based on re-evaluation of selected population members after perturbation in accordance with the prescribed uncertainty. For more details the reader can consult the referenced publications.

2.4 Workflow overview

The final workflow has the following steps:

1. Initial radial parameters x^k are specified as input
2. Perturbed parameters are sampled for λ members using the initial covariance matrix (eq. [5]).
3. For λ members, all WI_i values (eq. [1]) are calculated for the radial design characterised by the perturbed parameters.
4. For λ members, the reservoir simulation is performed using the WI_i values from step 3 resulting in the produced heat.
5. For λ members, NPV is calculated (eq. [2]).
6. The members are ranked according to the NPV.
7. Adapt mean parameter vector, covariance matrix and step size (eq. [3] – [5]) based on the best μ members.
8. Repeat from step 2, with the updated mean parameter vector instead of the initial parameters and the updated covariance matrix and step size.

For all experiments, 20 iterations were done in order to compare the performance.

3. EXPERIMENTS AND RESULTS

3.1 Case study overview

As a first step the workflow is tested on a relatively simple model of a single well in a reservoir with two high permeability layers, referred to as the '2-layer model'. The goal is to test the workflow. The second test case is also a single well model but now with thinly layered deposits. This model is based on the Klaipeda geothermal site (Nair et al., 2017). In the following the cases are described in more detail.

The 2-layer model has two high-permeable layers bounded on both sides by low-permeable rock (Figure 2). Details of the model are provided in Table 1. The vertical layering is chosen identical to the layering for the fine-layered model (Figure 3) which has more variation between thin zones with relatively low and high permeability.

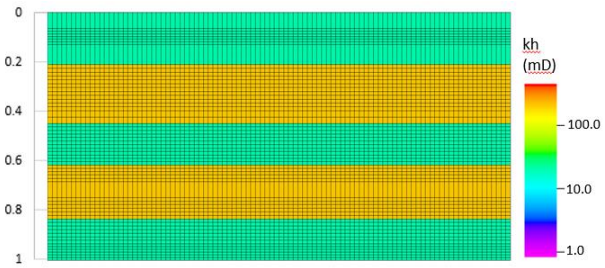

Figure 2: Cross-section of the 2-Layer model showing normalized depth and horizontal permeability k_h.

Table 1: Input for the 2-layer model

Grid	
Grid Cells (Ni x Nj x Nk)	100 x 100 x 59
dx x dy	10 m x 10 m
Depth interval	970 to 1125 m TVDSS
Rock properties (fine grid)	
k_h (high, low)	500 mD, 20 mD,
k_v	k_h / 5
Porosity	0.1
Net/Gross	1
Rock compressibility	0.00015 bar^{-1}
Initial Reservoir Conditions	
Pressure	107.2 bar @ -1047.5 m
Water Properties	
Density @ ref. conditions	1047 kg/m3
Viscosity	0.88 mPa·s
Formation Volume Factor	1.0004 rm^3/sm^3
Compressibility	0.000037 bar^{-1}

The fine-layered model is based on the geothermal reservoir at the Klaipėda geothermal site (Šliaupa, 2016; Brehme et al., 2017). The reservoir is composed of a fine-grained friable sandstone (fine and medium grained) from the Lower Devonian called the Kemeri Formation.

The reservoir has relatively thin layers with high permeability between thicker layers of fine grained material with lower permeability. The reservoir is developed with two injectors and two producers. Here only injector well 1I is used. Vertical layering is based on the facies distribution. The higher permeable layers have more detailed layering than the low permeable layers. Although the facies distribution is based on the logs from the well 1I, the permeability values have been chosen to make a suitable optimization case study Details of this model are provided in Table 2.

In both models we apply a constant pressure on the laterals boundary conditions and no-flow boundary conditions at the top and bottom of the model. In both cases a single producing well is positioned in the centre of the modelled domain.

Table 2: Input for the fine-layered model

Grid	
Grid Cells (Ni x Nj x Nk)	100 x 100 x 59
dx x dy	10 m x 10 m
Depth interval	970 to 1125 m TVDSS
Rock properties (fine grid)	
k_h (Coarse sand, fine sand, clay)	500 mD, 250 mD, 50 mD
kv (Coarse sand, fine sand, clay)	150 mD, 150 mD, 50 mD
Porosity (Coarse sand, fine sand, clay)	0.21, 0.14, 0.07
Rock compressibility	0.00015 bar^{-1}
Net/Gross	1
Initial Reservoir Conditions	
Pressure	120 bar @ -1047.5 m
Water Properties	
Density @ ref. conditions	1060 kg/m^3
Viscosity	0.88 mPa·s
Formation Volume Factor	1.0002 rm^3/sm^3
Compressibility	0.000036 bar^{-1}

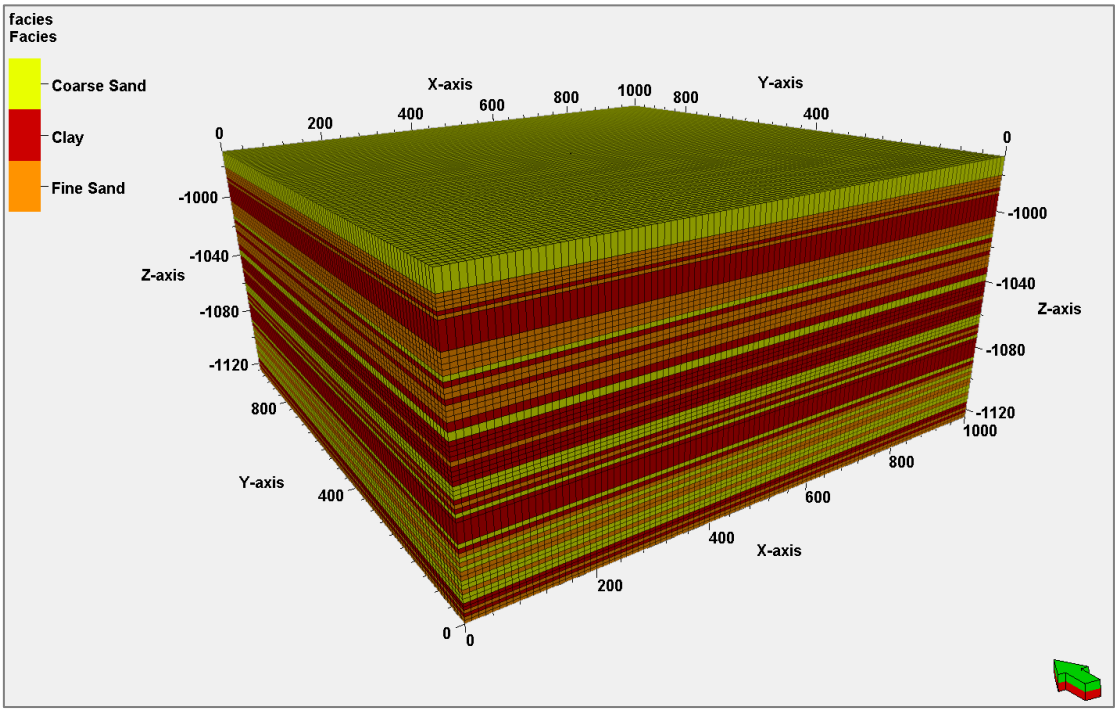

Figure 3: Geometry and facies distribution in the fine layered model

3.2 Results

Figure 4 shows the development of the performance measure or objective function (NPV) for the 2-layer case over 20 iterations for three different initial settings (see Table 3). Depth is scaled/normalized from 0 to 1 representing top and bottom of the reservoir respectively. The objective function value corresponds to the function evaluation of the mean control vector of the best μ members of the population. The depth of the kick-offs and the number of radials per kick-off were optimised. The number of kick-offs was fixed at 2. For all three cases, the NPV increases, although not to the same level (Figure 4). In this simple case, we can easily deduce what the optimal configuration is, namely one kick-off in the top high-permeability layer and one in the bottom high permeability layer. This is indeed the configuration found in two of the runs (Figure 5). However, in run 2, which has lower NPV, the two kick-offs have been placed in one of the two high-perm layers. Interference between the radials thus reduces the realized flow. Run 1 starts with a reasonably good initial guess and a smaller standard deviation for the initial sampling of perturbed kick-offs. Run 3 starts with a poorer initial guess, but larger standard deviation. The NPV for run 3 is the highest: in this run, the number of laterals is increased compared to run 1. The optimized kick-off depths are very similar for the two runs.

Table 3: Initial setting for the optimization of the 2-layer model: normalized kick-off depth and standard deviation σ of the kick-off depth.

Run	Kick-off depth 1	Kick-off depth 2	σ kick-off depth
1	0.3	0.6	0.2
2	0.5	0.9	0.2
3	0.5	0.9	0.3

In Figure 6 the NPVs of all population members which were simulated during the optimization process from run 3 are plotted as a function of the normalized kick-off depths. Despite the fact that also the number of laterals varies, the figure shows clearly at which depths the best performance is achieved. It also shows that part of the parameter space is not sampled, because the solution quickly converged towards the optimal values. For the other two runs, the distribution of the samples also didn't cover the entire parameter space. We have not attempted here to find the best tuning parameters for CMA-ES (e.g. the initial variances) that minimize simulation cost.

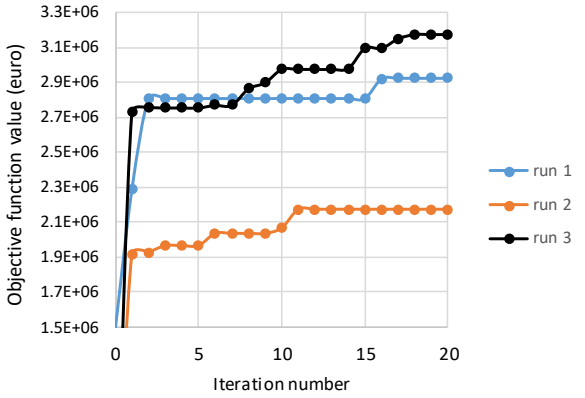

Figure 4: Development of NPV for the 2-Layer case during optimization of kick-off depth and number of radials.

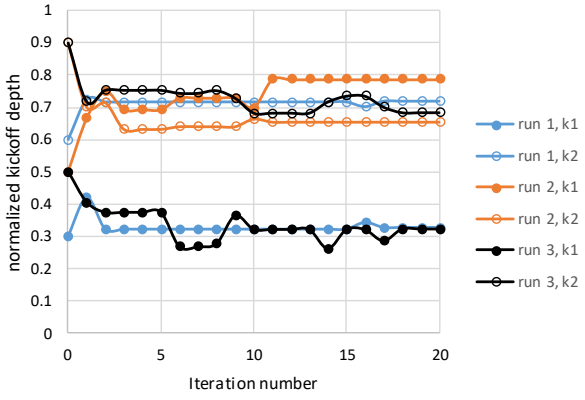

Figure 5: Development of kick-off depth in the accepted control vector (normalized between 0 and 1) for the 2-layer case during optimization.

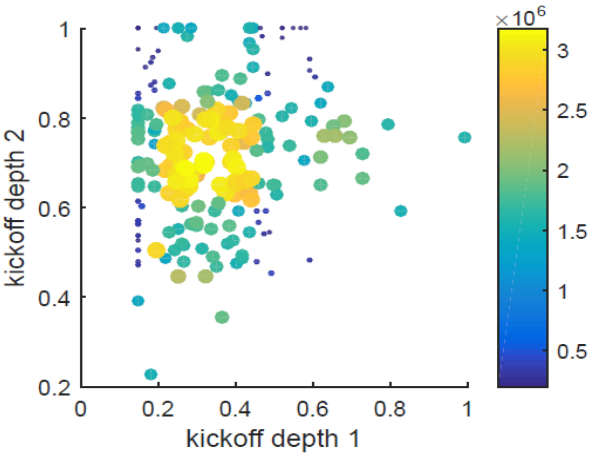

Figure 6: NPV as a function of normalized kick-off depth for the 2-Layer model with two kick-off points for all optimization runs.

The second model that was tested, the fine layered model, is a more challenging optimization problem, since there are multiple high permeability layers, as well as layers with intermediate permeability (see Figure 3). As in the 2-Layer case, the kick-off depth and the number of radials were optimized. Two optimization runs were done: one starting with two kick-off points and one with four kick-off points. The development of the objective function in Figure 7 shows that the convergence for the case with 2 kick-offs is faster, but the final NPV for 4 kick-offs is higher. Figures 8 and 9 show the evolution of the kick-off depth for the case with two kick-offs and the case with four kick-offs respectively. The depth value that is plotted is the mean kick-off depth of the μ best performing ensemble members. This is the also the depth used for the calculation of NPV plotted in Figure 7. In both cases, the kick-off points are moved to the coarse sand area in the bottom of the model with high permeability, except for one kick-off in the case with four kick-offs (Figure 9).

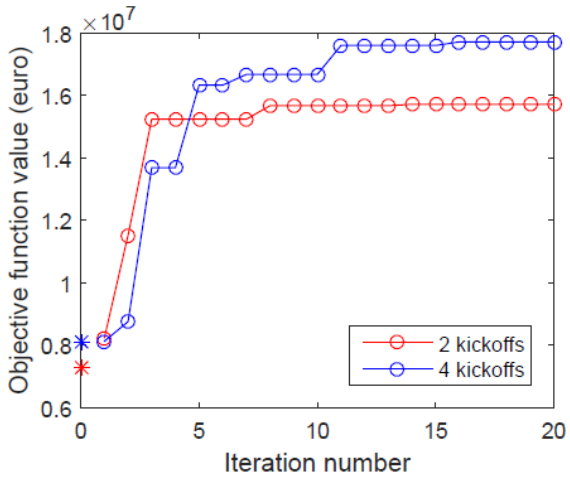

Figure 7: Development of NPV for the fine layered model for optimization with two and four kick-off points.

The number of radials is also optimized. The initial number of radials is four for all kick-offs independent or the number of kick-ffs. For the case with two kick-offs, the optimization results in more radials per kick-off (5 and 6) than in the case with four kick-offs (4 radials for most).

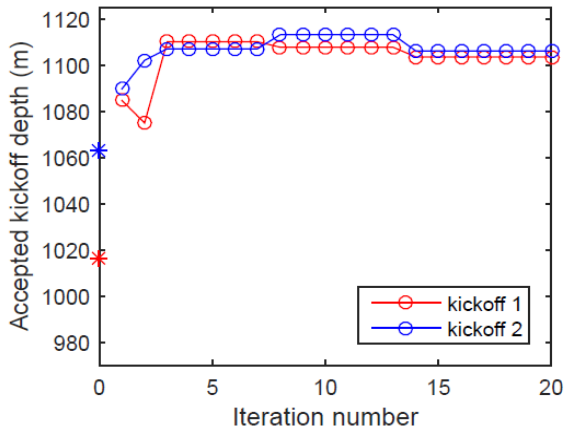

Figure 8: Development of the kick-off depths for the fine layered model with 2 kick-offs (stars indicate the initial values).

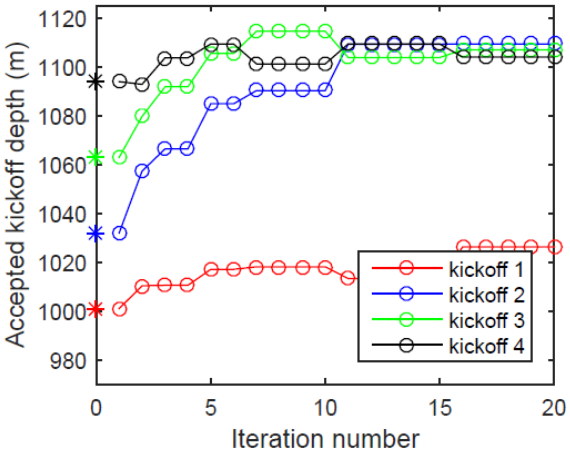

Figure 9: Development of the kick-off depth for the fine layered model for with 4 kick-offs (stars indicate the initial values).

From Figure 8 and Figure 9 it can be seen that the final designs are very different from the initial designs and that significantly improved designs can be found in a fairly limited number of iterations. To analyse whether a global optimum has been reached, in particular for the kick-off depth, the results of all population members were analysed. The best performing member for both cases had slightly higher NPV than the optimised mean. All NPV values encountered during optimization for the two kick-off case are plotted in Figure 10 as a function of normalized depth. The figure shows that indeed high NPV values are associated with larger depths for both kick-offs. From this figure it is clear that not the entire parameter space is sampled, similar to the 2-layer case. For the case with four kick-offs, sampling of the parameter space had better coverage, although also here, shallow depth values were under-represented.

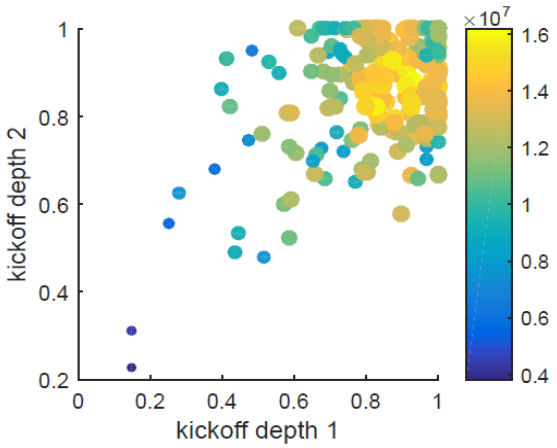

Figure 10: NPV as a function of normalized kick-off depth for the fine layered model for optimization with two kick-off points.

3.3 Uncertainty handling

Up until now, it was assumed that the radials are drilled in accordance with the design, i.e. that they have exactly the designed inclination and azimuth. Because the jetting nozzle cannot be steered, inclination and azimuth are highly uncertain in practice. For the fine-layered model, it is expected that in particular changes in inclination have impact on the results (Nair et al., 2017), because the radials can easily leave the high-perm layers. Therefore we have tested the optimization of the fine-layered model with a version of CMA-ES with uncertainty handling. Uncertainty was only assumed in the inclination of the radials. The standard deviation on the inclination was taken as 0.5π rad.

In Figure 11 the evolution of the objective function is plotted for both cases. The achieved NPV is a bit lower than for the normal CMA-ES. For the case with two kick-offs, the depths of the kick-offs (Figure 12) shows that one kick-off ended up in the area with high permeability in the lower part of the model and one in a zone with fine sands (medium permeability) around 1000 to 1020 m depth. In the case with four kick-offs (Figure 13), all kick-offs end up in the zone with high permeability at the bottom with three kick-offs almost in top of each other. The total number of radials for these three kick-offs together is 16, which means that 16 radials are almost at the same location. This almost certainly leads to interference between the radials, which is expected to be a sub-optimal solution. It is likely that the interference is less due to the uncertainty in the inclination of the radials, which increases the spread of the radials.

A more extensive analysis is required to fully understand the impact of the uncertainty handling on the optimization results.

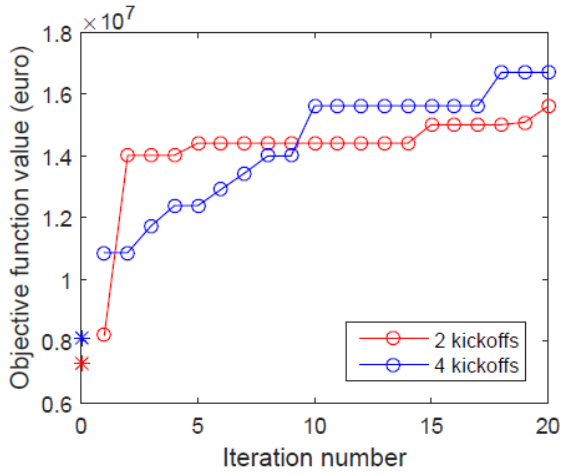

Figure 11: Development of NPV for the fine layered model with two kick-offs during optimization with uncertainty handling (stars indicate the initial values).

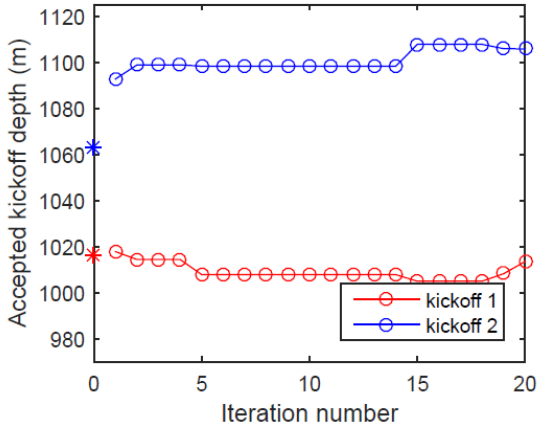

Figure 12: Development of kick-off depth for the fine layered model for optimization with uncertainty handling with two kick-offs (stars indicate the initial values).

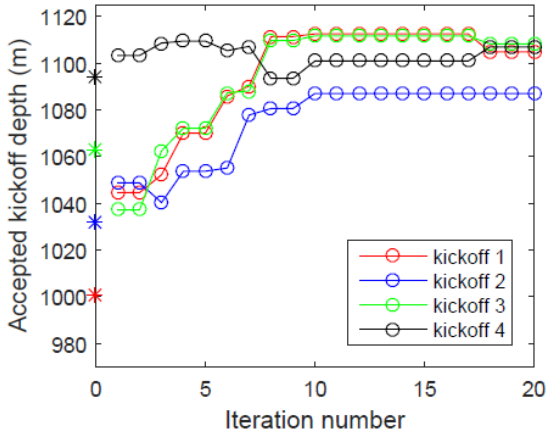

Figure 13: Development of kick-off depth for the fine layered model for optimization with uncertainty handling with four kick-offs (stars indicate the initial values).

4. CONCLUSIONS

In this study we have demonstrated the possibility of using numerical simulation models in conjunction with optimization algorithms to explore design options for stimulation of geothermal assets by radial jetting. The simulation model provides a quantitative and verifiable framework for evaluating different designs while the optimization algorithm enables systematic exploration and identification of the best possible design. The concept was first tested on a simple test case with a known optimal solution. After it was verified that the optimization workflow could indeed find the optimal solution, it was then applied to a single-well case with more realistic complexity in the distribution of rock properties. Also in this case, an improved placement of kick-offs and number of radials could be found.

A number of further improvements may be possible. In real settings, there will be a significant uncertainty associated with the rock properties in-between 2 wells of a geothermal doublet. This geological uncertainty could be incorporated in the optimization workflow, but possibly at a severe increase in computational cost. The treatment of uncertainty in the CMA-ES was tested here, but needs further analysis. Another variation that will be tested in the extension to integer variables proposed by Hansen (2011).

Most importantly, follow-up work will address more realistically complex design cases with doublets consisting of strongly deviated wells and geological heterogeneity.

REFERENCES

Barros, E., Chitu, A., and Leeuwenburgh, O.: Ensemble-based optimization of well trajectory design in the Olympus Field, EAGE/TNO Workshop on OLYMPUS Field Development Optimization, 7 September 2018, Barcelona, doi:10.3997/2214-4609.201802294.

Brehme, M., Blöcher, G., Regenspurg, S., Milsch, H., Petrauskas, S., Valickas, R., Wolfgramm, M. and Huenges, E.: Approach to develop a soft stimulation concept to overcome formation damage – A case study at Klaipeda, Lithuania. PROCEEDINGS, 42nd Workshop on Geothermal Reservoir Engineering, Stanford University, Stanford, California, 2017.

Hansen, N.: The CMA Evolution Strategy: A Tutorial, ArXiv e-prints, arXiv:1604.00772, 2016, pp.1-39.

Hansen, N, and Ostermeier, A.: Adapting arbitrary normal mutation distributions in evolution strategies: The covariance matrix adaptation. In Proceedings of the 1996 IEEE Conference on Evolutionary Computation (ICEC '96), pp. 312-317, 1996.

Hansen, N., The CMA Evolution Strategy: A Comparing Review, StudFuzz, 192, 75-102, 2006.

Hansen, N.: A CMA-ES for Mixed-Integer Nonlinear Optimization, [Research Report] RR-7751, INRIA. 2011. <inria-00629689>.

Hansen, N., Niederberger, A., Guzzella, L., and Koumoutsakos, P.: A Method for Handling Uncertainty in Evolutionary Optimization with an Application to Feedback Control of Combustion. IEEE Transactions on Evolutionary Computation, Institute of Electrical and Electronics Engineers, 2009. <inria-00276216>.

Kamel, A.H. 2017. A technical review of radial jet drilling. J. of Petroleum and Gas Eng. 8(8), (2017), 79-89. DOI: 10.5897/JPGE2017.0275

Lensink, S. (ed.) Eindadvies basisbedragen SDE+ 2019: 2018 https://www.pbl.nl/publicaties/eindadvies-basisbedragen-sde-2019.

Nair, R. Peters, E., Šliaupa, S., Valickas, R., Petrauskas, S.: A case study of radial jetting technology for enhancing geothermal energy systems at Klaipėda geothermal demonstration plant. PROCEEDINGS, 42nd Workshop on Geothermal Reservoir Engineering, Stanford University, Stanford, California, 2017.

NTNU, FieldOpt Well Index Calculator, code link stored at https://libraries.io/github/PetroleumCyberneticsGroup/FieldOpt-WellIndexCalculator. 2018.

Peters, E., Blöcher, G., Salimzadeh, S., Egberts, P.J.P., and Cacace, M.: Modelling of multi-lateral well geometries for geothermal applications. *Adv. Geosci.* **45**, (2018a) 209-215. https://doi.org/10.5194/adgeo-45-209-2018.

Peters, E., Egberts, P., Chitu, A., Nair, R., Salimzadeh, S., Blöcher, G. and Cacace, M.: The Horizon 2020 SURE Project: Deliverable 7.4 - Upscaling of RJD for incorporation in reservoir simulators, 2019, Potsdam : GFZ German Research Centre for Geosciences, DOI: 10.2312/gfz.4.8.2019.003.

Šliaupa, S.: Reservoir characterisation of the Klaipėda geothermal plant (Lithuania), Vilnius, Lithuania (2016). Nature Research Centre report.

Troost, D. Optimization of Jetted Radial Wells. MSc-thesis TUDelft, 2019.

Yan, J., Cui, M., He, A., Jiang, W. and Liang, C. Study and Application of Hydraulic Jet Radial Drilling in Carbonate Reservoirs. International Journal of Oil, Gas and Coal Engineering. Vol. 6, No. 5, (2018), pp. 96-101. doi: 10.11648/j.ogce.20180605.13.

Acknowledgements

The research for this paper received funding from the European Union's Horizon 2020 research and innovation programme under grant agreement No. 654662 (SURE). The content of this poster reflects only the authors' view. The Innovation and Networks Executive Agency (INEA) is not responsible for any use that may be made of the information it contains. The use of data from the Klaipėda site received from Geoterma is gratefully acknowledged. The help of NTNU with implementation of the WIC tool is gratefully acknowledged. The use of open source codes Field-Opt by NTNU and OPM-flow (https://opm-project.org/) is gratefully acknowledged.